NANO LETTERS

pubs.acs.org/NanoLett

Letter

Actively Tunable Metasurfaces via Plasmonic Nanogap Cavities with Sub-10-nm VO_2 Films

Andrew M. Boyce,[†] Jon W. Stewart,[†] Jason Avila, Qixin Shen, Siyuan Zhang, Virginia D. Wheeler, and Maiken H. Mikkelsen*

Cite This: *Nano Lett.* 2022, 22, 3525−3531

Read Online

ACCESS | Metrics & More | Article Recommendations | Supporting Information

ABSTRACT: Actively tunable optical materials integrated with engineered subwavelength structures could enable novel optoelectronic devices, including reconfigurable light sources and tunable on-chip spectral filters. The phase-change material vanadium dioxide (VO_2) provides a promising solid-state solution for dynamic tuning; however, previous demonstrations have been limited to thicker and often rough VO_2 films or require a lattice-matched substrate for growth. Here, sub-10-nm-thick VO_2 films are realized by atomic layer deposition (ALD) and integrated with plasmonic nanogap cavities to demonstrate tunable, spectrally selective absorption across 1200 nm in the near-infrared (NIR). Upon inducing the phase transition via heating, the absorption resonance is blue-shifted by as much as 60 nm. This process is reversible upon cooling and repeatable over more than ten temperature cycles. Dynamic, ultrathin VO_2 films deposited by ALD, as demonstrated here, open up new potential architectures and applications where VO_2 can be utilized to provide reconfigurability including three-dimensional, flexible and large-area structures.

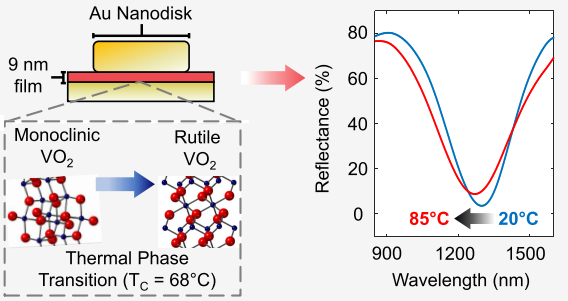

KEYWORDS: *plasmonics, nanocavity, nanoantenna, tunable metasurface, vanadium dioxide, phase transition*

Nanostructured optical materials have enabled unparalleled control over light−matter interactions for creating ultrafast single photon emitters,[1−3] efficient nonlinear surfaces,[4−7] and on-chip spectral filters.[8−10] Integration of active materials provides a means of tuning the optical properties in real-time promising for a new generation of multifunctional, nanoscale optoelectronic devices. Active metasurfaces have been demonstrated using a wide array of tuning mechanisms, including electrical modulation,[11−16] polarization of incident light,[17] mechanical strain,[18,19] hydrogen gas flow,[20,21] UV exposure,[22,23] femtosecond laser pulses,[24,25] and heating.[26−31] While there have been several demonstrations of robust tuning at mid-IR and longer wavelengths,[11,16,31] active metasurfaces in the visible and near-IR have generally been limited by tuning mechanisms that are ill-suited for practical devices, for reasons, such as lack of reversibility or degradation of switching over multiple cycles.[12,18,22,32] One option for overcoming these limitations is utilizing the phase-change material vanadium dioxide (VO_2), which offers robust switching via heating above 68 °C. At this temperature, VO_2 undergoes a first-order, crystalline phase transition with an accompanying change in its refractive index, which is fully reversible by cooling below the transition temperature.[33] It has also been reported that this phase change can be induced electrically with a less than 2 ns response time,[34] increasing the promise of VO_2 for integration into practical, active metasurface devices.

Previously, VO_2 has been used to create active metasurfaces over a broad wavelength range,[26,30,31,35−37] typically with bulk materials or sputtered films with thicknesses of 50−150 nm[38−43] or more rarely by utilizing a lattice-matched substrate for growth of thinner films.[44] However, integrating nanometer-scale VO_2 films with nanocavity structures on non-lattice-matched substrates has remained an outstanding challenge, yet offers the promise for robust, deeply subwavelength tunable optoelectronic devices to enable, for example, nanoscale optical memories and dynamic control of quantum emitters. Furthermore, conventional techniques to deposit VO_2 thin films, such as pulsed laser deposition (PLD), are only uniform over small areas, do not deposit conformally and are incompatible with many materials. ALD provides a promising, alternative deposition technique that enables highly uniform films over wafer-scale areas, conformal coating of three-dimensional or flexible structures as well as integration of dissimilar materials that can be deposited with abrupt interfaces. Lastly, the resultant ultrathin layers may allow for

Received: October 28, 2021
Revised: March 20, 2022
Published: April 26, 2022

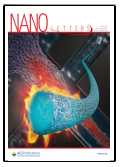

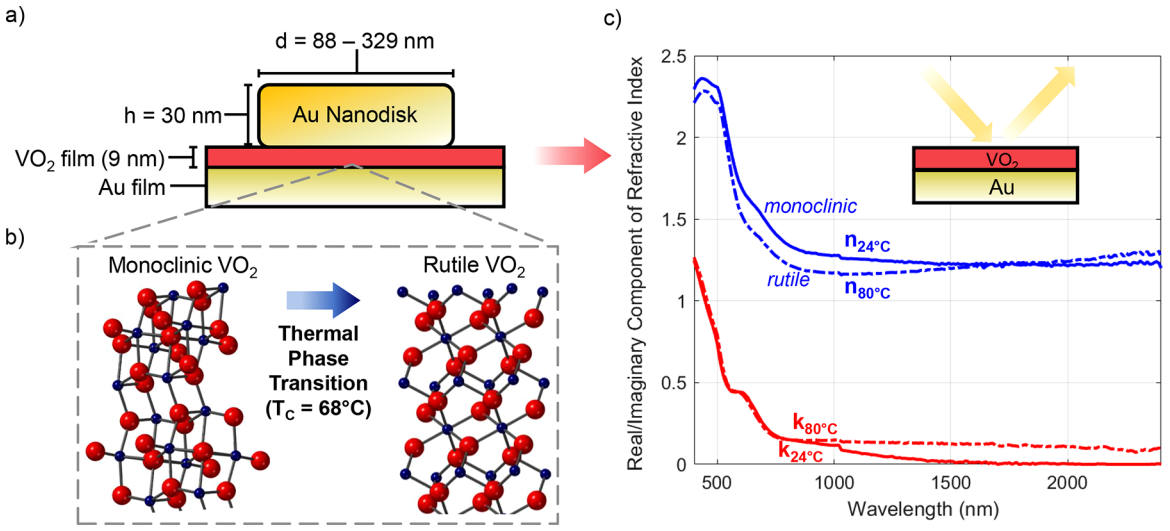

Figure 1. (a) Schematic of sample structure consisting of Au nanodisks (height = 30 nm) separated from an Au ground plane by 9 nm of VO_2. (b) Illustration of the phase transition of VO_2. Upon heating to ~68 °C, the crystal structure shifts from monoclinic to rutile leading to a corresponding change in its refractive index. (c) Ellipsometry-measured real and imaginary components of the refractive index of a 9 nm VO_2 film on Au at room temperature and after heating to 80 °C. This data is plotted in terms of the real and imaginary components of ε in Figure S1.

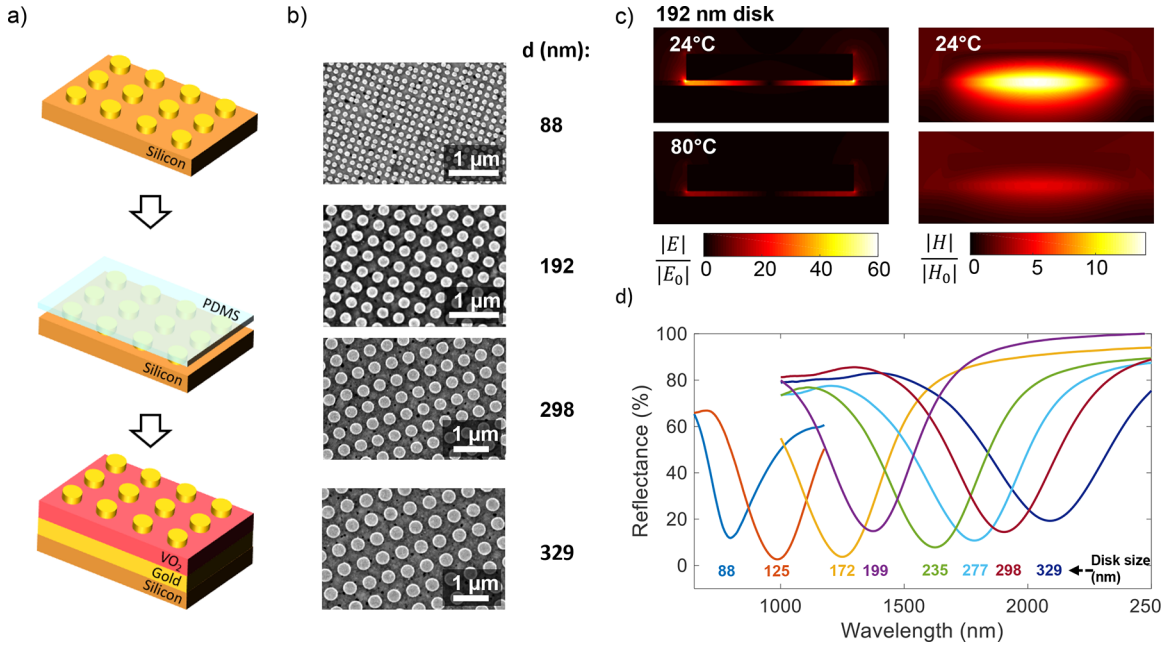

Figure 2. (a) Fabrication process for transferring EBL-fabricated gold nanodisks onto the VO_2 film. (b) SEM images of gold nanodisks for a few of the fabricated sizes. (c) Simulated electric (left) and magnetic (right) field profiles at 24 and 80 °C for the nanogap cavity structure with 192 nm gold nanodisks. An incident plane wave with wavelength matching the room-temperature resonance of the nanocavity at 1495 nm is utilized. (d) Room-temperature reflectance spectra for metasurfaces consisting of eight different sizes of nanodisks where additional spectra are shown in Figure S4.

heat to be removed faster which could enable devices with a faster thermal response.

Here, we demonstrate reversible tuning of near-IR absorption resonances from active plasmonic metasurfaces via the insulator-to-metal phase transition of a 9 nm VO_2 film grown by ALD. The tunable metasurfaces consist of arrays of plasmonic nanodisks on top of the VO_2 and Au films, where a single nanocavity is shown in Figure 1a. The parallel metallic interfaces in Figure 1a create a planar cavity between the two Au surfaces separated by the VO_2 film, which supports a gap-mode surface plasmon.[45] The resonance wavelength is determined by the geometry, material, and refractive index of the constituent nanocavity elements.[46−49]

The resonances are statically controlled by varying the nanoparticle diameter and dynamically controlled through the refractive index tuning of the VO_2 layer. Upon heating to ~68 °C, VO_2 undergoes a phase transition which alters the corresponding crystal structure from monoclinic to rutile as depicted in Figure 1b. In the monoclinic phase, VO_2 is transparent and insulating in the IR and possesses a bandgap of 0.7 eV.[50] When transitioned to the tetragonal phase, the bandgap closes resulting in lossy metallic behavior or a metallic

https://doi.org/10.1021/acs.nanolett.1c04175
Nano Lett. 2022, 22, 3525−3531

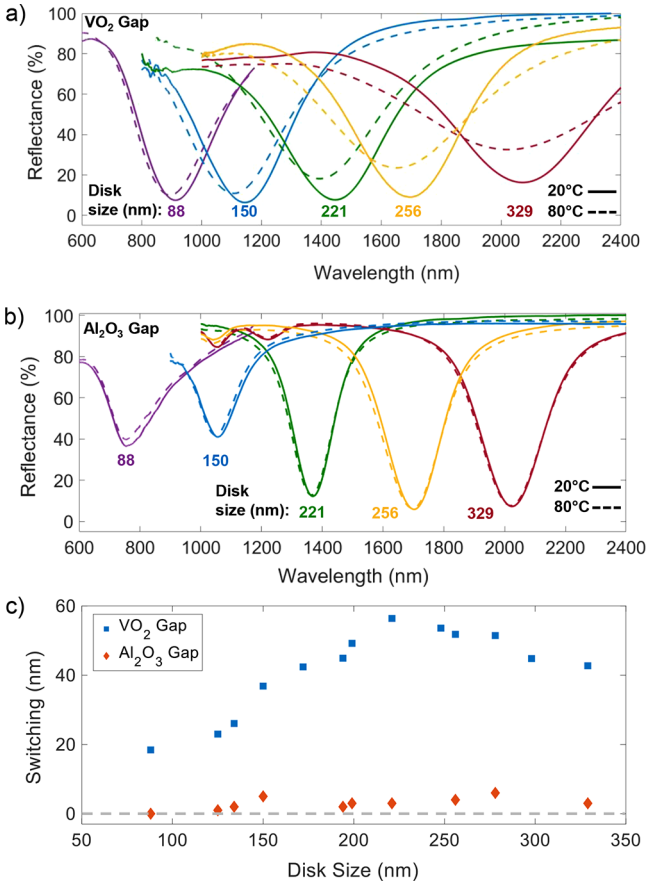

Figure 3. (a) Thermal switching spectra for metasurfaces consisting of 88, 150, 221, 256, and 329 nm diameter Au nanodisks. Spectra for the remaining sizes are shown in Figure S5. (b) Switching spectra from a control sample with a gap consisting of 9 nm of Al_2O_3 for the same size nanodisks as in panel a. (c) Comparison of the amount of switching observed experimentally for both the control sample (9 nm Al_2O_3 gap) and the VO_2 thermal switching sample (9 nm VO_2 gap). The gray dashed line at 0 nm of switching is intended to guide the reader's eye.

phase. Beyond a purely electronic transition, this insulator-to-metal transition possesses a concomitant change in the real and imaginary components of the refractive index. Figure 1c depicts the refractive index change for a 9 nm film deposited on Au and measured by ellipsometry at 24 and 80 °C for wavelengths spanning from 400 to 2400 nm. Spectrally, the largest refractive index change of −0.17 occurs at 640 nm for the real component and 0.12 at 1660 nm for the imaginary component. In the monoclinic phase, the VO_2 film exhibits normal dispersion for wavelengths longer than 500 nm indicative of the insulating or dielectric state. When in the tetragonal phase at 80 °C, the refractive index shows anomalous dispersion at wavelengths longer than 1000 nm indicative of metallic behavior. As such, the refractive index change in Figure 1c distinctly shows the insulator-to-metal transition induced upon heating. Although the real component of the permittivity of the VO_2 film is expected to go below zero around the plasma frequency, and this has been demonstrated previously for VO_2 films fabricated in a similar manner,[51] this behavior is not observed in the present samples and can likely be explained by the ultrathin nature of the VO_2 film and the underlying nonlattice-matched gold substrate.

Fabrication of the structure began with growing the VO_2 on a 75 nm-thick Au film via ALD according to a process that has been extensively characterized elsewhere and been shown to produce thin films capable of undergoing a phase change[52−54] Subsequently, the sample was annealed to form a poly crystalline film from the initially amorphous material and had the effect of ensuring that the metasurface switching was fully reversible (details in methods section). X-ray photoelectron spectroscopy (XPS) characterization of the annealed VO_2 films was performed (shown in Figure S2) and revealed V^{+4} and V^{+5} peaks with full-widths at half-maximum (fwhm) of around 1.6−1.7 eV, indicating that the film has a fairly high degree of crystallinity as amorphous films typically have widths around 2−3 eV due to slight variations in bonding strengths. While the V^{+4} peak is indicative of a VO_2 film, the V^{+5} peak is the result of some undesired contamination, likely in the form of a hydroxyl group or V−O−C bonding in addition to the V_2O_5 stoichiometry. However, previous studies have determined that the thickness of this contaminated layer is no more than 1 nm and results from the subsequent fabrication steps being performed in atmospheric conditions.[53] SEM images of the VO_2 film (shown in Figure S3) reveal the presence of pinholes that likely have the effect of reducing the amount of switching that can be achieved. However, such defects are common for depositions on a non-lattice-matched and polycrystalline substrate.

Next, the VO_2 films were embedded into plasmonic nanocavities by transferring Au nanodisks on top of them. The Au nanodisks were fabricated using electron-beam lithography (EBL) on a Si substrate. Because of the weak adhesion of Au to the Si substrate, the Au nanodisks could be exfoliated from the Si wafer after removing the native SiO_2 and deposited onto the VO_2 film using a PDMS stamp as shown in Figure 2a. This technique was utilized because of the sensitivity of VO_2 to electron-beam exposures and subsequent development processes (additional fabrication details in SI). In all, 13 metasurfaces were fabricated by varying the diameter of the nanodisks (from 88 to 329 nm), where SEM images of representative metasurfaces are shown in Figure 2b. The plasmonic nanocavities possess a large effective electric and magnetic response on resonance as shown in Figure 2c, which is strongly localized in the VO_2 film below the disks. As such, a sufficient fill fraction of nanocavities on the surface can result in near-perfect absorption at the plasmon resonance because of the large absorption cross section of each individual antenna element resulting in near-total effective surface coverage and absorption of incident light. Alternatively, this can be thought of as the destructive interference of the reflected wave with the multitude of plasmonic modes.[46,49]

Because of the spectrally dependent variations in the insulator-to-metal transition, 13 spectrally distinct metasurfaces were used to assess the dispersion of the active tuning. The resonant wavelengths for these absorbing metasurfaces range from ∼900 to 2100 nm and span above and below the anomalous dispersion of the tetragonal VO_2 phase. The room-temperature reflection spectra of the metasurfaces were measured with a white light source focused through a 0.4 NA objective as shown in Figure 2d (additional spectra in Figure S4). All the metasurfaces demonstrate near-perfect absorption of incident light on resonance, with typical peak absorption values of ∼95%. The switching spectra for the 88, 150, 221, 256, and 329 nm nanodisk metasurfaces are shown in Figure 3a, while switching spectra for the remaining sizes are

https://doi.org/10.1021/acs.nanolett.1c04175
Nano Lett. 2022, 22, 3525−3531

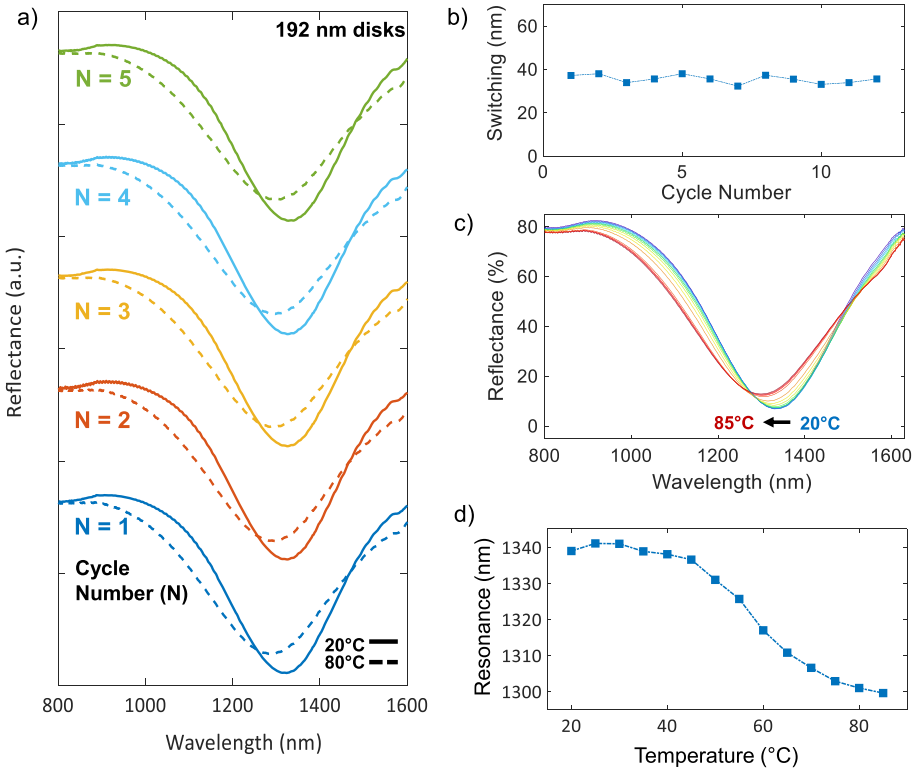

Figure 4. Characteristics of thermal switching for a metasurface consisting of 192 nm gold nanodisks. (a) Thermal switching spectra over five cycles, which shows fully reversible switching. (b) Magnitude of switching over 12 cycles of the temperature. (c) Switching spectra over one heating cycle taken in 5 °C increments from 20 to 85 °C. (d) Extracted resonance wavelength as a function of temperature for the spectra displayed in panel c.

shown in Figure S5. In addition to producing a spectral shift in the resonance, heating the metasurfaces was also observed to modulate the peak absorbance by as much as 16%, contributing further to the dynamic nature of this structure.

A control sample was also fabricated with a gap comprised of a non-phase-change material (9 nm of Al_2O_3). The thermal switching spectra for select sizes of nanodisks on this sample (same sizes as shown in Figure 3a) are presented in Figure 3b. An average of only 3 nm of wavelength switching was observed for the control sample. A comparison of the amount of switching for each nanodisk size for both the sample with the VO_2 gap and the sample with the Al_2O_3 gap is shown in Figure 3c. We note that the full-width at half-maximum (fwhm) of the resonance on the control sample is less for the control sample. This is likely due to increased surface roughness for the VO_2 film arising from the annealing process which resulted in larger inhomogeneous broadening of the plasmon resonance.

To provide additional insight into the spectral dependence of the switching behavior, the active metasurfaces were simulated with a finite-difference solver to model the temperature-dependent reflection spectra for the various metasurfaces. The simulated spectra for the same sizes of nanodisks as in Figure 3a are shown in Supporting Figure 6. Both the simulations and experimental results show that spectral switching can be maximized for a given geometry and resonant wavelength. Furthermore, simulations show good agreement with experiment in terms of the magnitude of thermal switching that is predicted, although, for some disk sizes, simulations predict a different direction for the switching than what is observed experimentally.

For further characterization of the VO_2 switching, the amount of switching for the 192 nm nanodisks metasurface is analyzed over multiple cycles and smaller temperature steps. The temperature-dependent reflectance spectra of the 192 nm nanodisk metasurface over five cycles is shown in Figure 4a. In all, reflection spectra for this metasurface were collected over 12 temperature cycles; the shift in peak wavelength measured during each cycle is plotted in Figure 4b instead of the full spectra for clarity. For each cycle, the magnitude of shift was observed to be 36 ± 2 nm, demonstrating the repeatable nature of the thermal switching. The reflection spectra of the 192 nm nanodisk metasurface was also measured at 5 °C increments to characterize the continuity of the switching in more detail, and the results are shown in Figure 4c. The extracted resonance wavelength is shown as a function of temperature in Figure 4d. The resonance wavelength of the 192 nm metasurface displays little change until the temperature approaches 45 °C. The resonance then begins to blue-shift with increasing temperature, reaching a maximum rate of change at 60 °C. This implies a transition temperature of ∼60 °C for the fabricated VO_2 gap layer, which is slightly less than the reported value in literature for bulk VO_2.[33] Previous investigations of ALD-grown VO_2 have similarly shown a lowered transition temperature of 61 °C.[53] Above 80 °C in our experiments, the resonance wavelength stabilizes at a final value of 1300 nm, which is blue-shifted by 40 nm compared to the resonance wavelength at room temperature. The lowered transition temperature and gradual phase shift occurring over a 40 °C range when compared to bulk VO_2 is characteristic of the effect of boundary conditions on the VO_2 thin films. The amount of switching observed here is less than what has been

https://doi.org/10.1021/acs.nanolett.1c04175
Nano Lett. 2022, 22, 3525−3531

measured previously with sputtered/PLD VO_2 films or bulk material and likely arises from a combination of the effects of interface strain on the ultrathin film and the presence of only a small amount of the phase-change material. Further optimization of the VO_2 film deposition process on an Au substrate, such as reducing the roughness and Au dewetting that occur during annealing as well as lessening contamination in the form of V^{+5}, is expected to lead to a larger tuning range.

In summary, we have demonstrated thermally tunable nanogap absorbers, which rely upon a robust, solid-state switching mechanism and possess a range of resonant wavelengths spanning 1200 nm in the near-IR. These metasurfaces display up to 60 nm of switching that is fully reversible over more than 10 temperature cycles. With the current amount of switching, we anticipate that this structure could be utilized for controllable enhancement of processes such as fluorescence, single photon emission, and nonlinear generation, as these effects depend strongly on the overlap of the resonance with the wavelength of the process of interest.[6,55] An additional application that should be realizable with the current amount of switching is holography since the phase of the reflection coefficient varies rapidly around the resonance wavelength. Thus, a modest shift in the resonance wavelength should lead to a large shift in phase. With improvements to the VO_2 thin film deposition, such that the magnitude of switching is increased, a variety of additional deeply subwavelength, all-solid-state, optoelectronic devices could be created using this platform including optical switches and memories, tunable photodetectors, and reconfigurable displays.

■ ASSOCIATED CONTENT

Supporting Information

The Supporting Information is available free of charge at https://pubs.acs.org/doi/10.1021/acs.nanolett.1c04175.

> Temperature-dependent ellipsometry data plotted in terms of the real and imaginary components of epsilon, details on the fabrication method, X-ray photoelectron spectroscopy (XPS) spectra of the VO_2 films, additional SEM images of the metasurface, room-temperature and thermal-switching spectra for the nanodisk sizes not shown in the main text, and simulated thermal switching spectra (PDF)

■ AUTHOR INFORMATION

Corresponding Author

Maiken H. Mikkelsen − *Department of Electrical and Computer Engineering and Department of Physics, Duke University, Durham, North Carolina 27708, United States;* orcid.org/0000-0002-0487-7585; Email: m.mikkelsen@duke.edu

Authors

Andrew M. Boyce − *Department of Electrical and Computer Engineering, Duke University, Durham, North Carolina 27708, United States*

Jon W. Stewart − *Department of Electrical and Computer Engineering, Duke University, Durham, North Carolina 27708, United States*

Jason Avila − *U.S. Naval Research Laboratory, Washington, D.C. 20375, United States*

Qixin Shen − *Department of Physics, Duke University, Durham, North Carolina 27708, United States*

Siyuan Zhang − *Department of Electrical and Computer Engineering, Duke University, Durham, North Carolina 27708, United States*

Virginia D. Wheeler − *U.S. Naval Research Laboratory, Washington, D.C. 20375, United States;* orcid.org/0000-0002-6024-9516

Complete contact information is available at: https://pubs.acs.org/10.1021/acs.nanolett.1c04175

Author Contributions

†A.M.B. and J.W.S. contributed equally to this work.

Notes

The authors declare no competing financial interest.

■ ACKNOWLEDGMENTS

M.H.M. acknowledges support from the Office of Naval Research (ONR) award no. N00014-17-1-2589, the Army Research Office (ARO) award no. W911NF1610471, and the Air Force Office of Scientific Research (AFOSR) award no. FA9550-18-1-0326 and FA9550-21-1-0312. V.D.W. acknowledges support from the Office of Naval Research (ONR). J.A. acknowledges support from the American Society of Engineering Education (ASEE).

■ REFERENCES

(1) Bracher, D. O.; Zhang, X.; Hu, E. L. Selective Purcell Enhancement of Two Closely Linked Zero-Phonon Transitions of a Silicon Carbide Color Center. *Proc. Natl. Acad. Sci. U. S. A.* **2017**, *114* (16), 4060−4065.

(2) Hoang, T. B.; Akselrod, G. M.; Mikkelsen, M. H. Ultrafast Room-Temperature Single Photon Emission from Quantum Dots Coupled to Plasmonic Nanocavities. *Nano Lett.* **2016**, *16* (1), 270−275.

(3) Luo, Y.; Shepard, G. D.; Ardelean, J. V.; Rhodes, D. A.; Kim, B.; Barmak, K.; Hone, J. C.; Strauf, S. Deterministic Coupling of Site-Controlled Quantum Emitters in Monolayer WSe_2 to Plasmonic Nanocavities. *Nat. Nanotechnol.* **2018**, *13* (12), 1137−1142.

(4) Aouani, H.; Rahmani, M.; Navarro-Cía, M.; Maier, S. A. Third-Harmonic-Upconversion Enhancement from a Single Semiconductor Nanoparticle Coupled to a Plasmonic Antenna. *Nat. Nanotechnol.* **2014**, *9* (4), 290−294.

(5) Zhang, Y.; Wen, F.; Zhen, Y. R.; Nordlander, P.; Halas, N. J. Coherent Fano Resonances in a Plasmonic Nanocluster Enhance Optical Four-Wave Mixing. *Proc. Natl. Acad. Sci. U. S. A.* **2013**, *110* (23), 9215−9219.

(6) Shen, Q.; Hoang, T. B.; Yang, G.; Wheeler, V. D.; Mikkelsen, M. H. Probing the Origin of Highly-Efficient Third-Harmonic Generation in Plasmonic Nanogaps. *Opt. Express* **2018**, *26* (16), 20718.

(7) Nielsen, M. P.; Shi, X.; Dichtl, P.; Maier, S. A.; Oulton, R. F. Giant Nonlinear Response at a Plasmonic Nanofocus Drives Efficient Four Wave Mixing over Micron Length Scales. *Science (80-.)* **2017**, *358* (6367), 1179−1181.

(8) Walter, R.; Tittl, A.; Berrier, A.; Sterl, F.; Weiss, T.; Giessen, H. Large-Area Low-Cost Tunable Plasmonic Perfect Absorber in the near Infrared by Colloidal Etching Lithography. *Adv. Opt. Mater.* **2015**, *3* (3), 398−403.

(9) Sturmberg, B. C. P.; Chong, T. K.; Choi, D.-Y.; White, T. P.; Botten, L. C.; Dossou, K. B.; Poulton, C. G.; Catchpole, K. R.; McPhedran, R. C.; Martijn de Sterke, C. Total Absorption of Visible Light in Ultrathin Weakly Absorbing Semiconductor Gratings. *Optica* **2016**, *3* (6), 556.

(10) Teperik, T. V.; García De Abajo, F. J.; Borisov, A. G.; Abdelsalam, M.; Bartlett, P. N.; Sugawara, Y.; Baumberg, J. J.

Omnidirectional Absorption in Nanostructured Metal Surfaces. *Nat. Photonics* **2008**, *2* (5), 299−301.
(11) Huang, Y. W.; Lee, H. W. H.; Sokhoyan, R.; Pala, R. A.; Thyagarajan, K.; Han, S.; Tsai, D. P.; Atwater, H. A. Gate-Tunable Conducting Oxide Metasurfaces. *Nano Lett.* **2016**, *16* (9), 5319−5325.
(12) Hoang, T. B.; Mikkelsen, M. H. Broad Electrical Tuning of Plasmonic Nanoantennas at Visible Frequencies. *Appl. Phys. Lett.* **2016**, *108* (18).183107
(13) Peng, J.; Jeong, H. H.; Lin, Q.; Cormier, S.; Liang, H. L.; De Volder, M. F. L.; Vignolini, S.; Baumberg, J. J. Scalable Electrochromic Nanopixels Using Plasmonics. *Sci. Adv.* **2019**, *5* (5), eaaw2205.
(14) König, T. A. F.; Ledin, P. A.; Kerszulis, J.; Mahmoud, M. A.; El-Sayed, M. A.; Reynolds, J. R.; Tsukruk, V. V. Electrically Tunable Plasmonic Behavior of Nanocube-Polymer Nanomaterials Induced by a Redox-Active Electrochromic Polymer. *ACS Nano* **2014**, *8* (6), 6182−6192.
(15) Xiong, K.; Tordera, D.; Emilsson, G.; Olsson, O.; Linderhed, U.; Jonsson, M. P.; Dahlin, A. B. Switchable Plasmonic Metasurfaces with High Chromaticity Containing Only Abundant Metals. *Nano Lett.* **2017**, *17* (11), 7033−7039.
(16) Yao, Y.; Kats, M. A.; Genevet, P.; Yu, N.; Song, Y.; Kong, J.; Capasso, F. Broad Electrical Tuning of Graphene-Loaded Plasmonic Antennas. *Nano Lett.* **2013**, *13* (3), 1257−1264.
(17) Franklin, D.; Frank, R.; Wu, S. T.; Chanda, D. Actively Addressed Single Pixel Full-Colour Plasmonic Display. *Nat. Commun.* **2017**, *8*, 15209.
(18) Gutruf, P.; Zou, C.; Withayachumnankul, W.; Bhaskaran, M.; Sriram, S.; Fumeaux, C. Mechanically Tunable Dielectric Resonator Metasurfaces at Visible Frequencies. *ACS Nano* **2016**, *10* (1), 133−141.
(19) Huang, F.; Baumberg, J. J. Actively Tuned Plasmons on Elastomerically Driven Au Nanoparticle Dimers. *Nano Lett.* **2010**, *10* (5), 1787−1792.
(20) Duan, X.; Kamin, S.; Liu, N. Dynamic Plasmonic Colour Display. *Nat. Commun.* **2017**, *8*, 14606.
(21) Strohfeldt, N.; Tittl, A.; Schäferling, M.; Neubrech, F.; Kreibig, U.; Griessen, R.; Giessen, H. Yttrium Hydride Nanoantennas for Active Plasmonics. *Nano Lett.* **2014**, *14* (3), 1140−1147.
(22) Wilson, W. M.; Stewart, J. W.; Mikkelsen, M. H. Surpassing Single Line Width Active Tuning with Photochromic Molecules Coupled to Plasmonic Nanoantennas. *Nano Lett.* **2018**, *18* (2), 853−858.
(23) Shao, L.; Zhuo, X.; Wang, J. Advanced Plasmonic Materials for Dynamic Color Display. *Adv. Mater.* **2018**, *30* (16), 1704338.
(24) Michel, A. K. U.; Zalden, P.; Chigrin, D. N.; Wuttig, M.; Lindenberg, A. M.; Taubner, T. Reversible Optical Switching of Infrared Antenna Resonances with Ultrathin Phase-Change Layers Using Femtosecond Laser Pulses. *ACS Photonics* **2014**, *1* (9), 833−839.
(25) Yang, Y.; Kelley, K.; Sachet, E.; Campione, S.; Luk, T. S.; Maria, J. P.; Sinclair, M. B.; Brener, I. Femtosecond Optical Polarization Switching Using a Cadmium Oxide-Based Perfect Absorber. *Nat. Photonics* **2017**, *11* (6), 390−395.
(26) Kats, M. A.; Blanchard, R.; Genevet, P.; Yang, Z.; Qazilbash, M. M.; Basov, D. N.; Ramanathan, S.; Capasso, F. Thermal Tuning of Mid-Infrared Plasmonic Antenna Arrays Using a Phase Change Material. *Opt. Lett.* **2013**, *38* (3), 368.
(27) Huang, J.; Traverso, A. J.; Yang, G.; Mikkelsen, M. H. Real-Time Tunable Strong Coupling: From Individual Nanocavities to Metasurfaces. *ACS Photonics* **2019**, *6* (4), 838−843.
(28) Sautter, J.; Staude, I.; Decker, M.; Rusak, E.; Neshev, D. N.; Brener, I.; Kivshar, Y. S. Active Tuning of All-Dielectric Metasurfaces. *ACS Nano* **2015**, *9* (4), 4308−4315.
(29) Yin, X.; Steinle, T.; Huang, L.; Taubner, T.; Wuttig, M.; Zentgraf, T.; Giessen, H. Beam Switching and Bifocal Zoom Lensing Using Active Plasmonic Metasurfaces. *Light Sci. Appl.* **2017**, *6* (7), e17016−e17016.
(30) Rensberg, J.; Zhang, S.; Zhou, Y.; McLeod, A. S.; Schwarz, C.; Goldflam, M.; Liu, M.; Kerbusch, J.; Nawrodt, R.; Ramanathan, S.; Basov, D. N.; Capasso, F.; Ronning, C.; Kats, M. A. Active Optical Metasurfaces Based on Defect-Engineered Phase-Transition Materials. *Nano Lett.* **2016**, *16* (2), 1050−1055.
(31) Driscoll, T.; Palit, S.; Qazilbash, M. M.; Brehm, M.; Keilmann, F.; Chae, B. G.; Yun, S. J.; Kim, H. T.; Cho, S. Y.; Jokerst, N. M.; Smith, D. R.; Basov, D. N. Dynamic Tuning of an Infrared Hybrid-Metamaterial Resonance Using Vanadium Dioxide. *Appl. Phys. Lett.* **2008**, *93* (2).024101
(32) Wang, G.; Chen, X.; Liu, S.; Wong, C.; Chu, S. Mechanical Chameleon through Dynamic Real-Time Plasmonic Tuning. *ACS Nano* **2016**, *10* (2), 1788−1794.
(33) Chain, E. E. Optical Properties of Vanadium Dioxide and Vanadium Pentoxide Thin Films. *Appl. Opt.* **1991**, *30* (19), 2782−2787.
(34) Zhou, Y.; Chen, X.; Ko, C.; Yang, Z.; Mouli, C.; Ramanathan, S. Voltage-Triggered Ultrafast Phase Transition in Vanadium Dioxide Switches. *IEEE Electron Device Lett.* **2013**, *34* (2), 220−222.
(35) Kocer, H.; Butun, S.; Banar, B.; Wang, K.; Tongay, S.; Wu, J.; Aydin, K. Thermal Tuning of Infrared Resonant Absorbers Based on Hybrid Gold-VO2 Nanostructures. *Appl. Phys. Lett.* **2015**, *106*, 161104.
(36) Song, Z.; Wang, K.; Li, J.; Liu, Q. H. Broadband Tunable Terahertz Absorber Based on Vanadium Dioxide Metamaterials. *Opt. Express* **2018**, *26* (6), 7148.
(37) Wang, S.; Kang, L.; Werner, D. H. Hybrid Resonators and Highly Tunable Terahertz Metamaterials Enabled by Vanadium Dioxide (VO2). *Sci. Rep.* **2017**, *7* (1), 4326.
(38) Xu, G.; Chen, Y.; Tazawa, M.; Jin, P. Surface Plasmon Resonance of Silver Nanoparticles on Vanadium Dioxide. *J. Phys. Chem. B* **2006**, *110* (5), 2051−2056.
(39) Shu, F. Z.; Yu, F. F.; Peng, R. W.; Zhu, Y. Y.; Xiong, B.; Fan, R. H.; Wang, Z. H.; Liu, Y.; Wang, M. Dynamic Plasmonic Color Generation Based on Phase Transition of Vanadium Dioxide. *Adv. Opt. Mater.* **2018**, *6* (7), 1700939.
(40) Kakiuchida, H.; Jin, P.; Nakao, S.; Tazawa, M. Optical Properties of Vanadium Dioxide Film during Semiconductive-Metallic Phase Transition. *Jpn. J. Appl. Phys.* **2007**, *46*, L113.
(41) Earl, S. K.; James, T. D.; Davis, T. J.; McCallum, J. C.; Marvel, R. E.; Haglund, R. F.; Roberts, A. Tunable Optical Antennas Enabled by the Phase Transition in Vanadium Dioxide. *Opt. Express* **2013**, *21* (22), 27503.
(42) Dicken, M. J.; Aydin, K.; Pryce, I. M.; Sweatlock, L. A.; Boyd, E. M.; Walavalkar, S.; Ma, J.; Atwater, H. A. Frequency Tunable Near-Infrared Metamaterials Based on VO_2 Phase Transition. *Opt. Express* **2009**, *17* (20), 18330.
(43) Muskens, O. L.; Bergamini, L.; Wang, Y.; Gaskell, J. M.; Zabala, N.; De Groot, C. H.; Sheel, D. W.; Aizpurua, J. Antenna-Assisted Picosecond Control of Nanoscale Phase Transition in Vanadium Dioxide. *Light Sci. Appl.* **2016**, *5* (10), e16173−9.
(44) Peter, A. P.; Martens, K.; Rampelberg, G.; Toeller, M.; Ablett, J. M.; Meersschaut, J.; Cuypers, D.; Franquet, A.; Detavernier, C.; Rueff, J. P.; Schaekers, M.; Van Elshocht, S.; Jurczak, M.; Adelmann, C.; Radu, I. P. Metal-Insulator Transition in ALD VO_2 Ultrathin Films and Nanoparticles: Morphological Control. *Adv. Funct. Mater.* **2015**, *25* (5), 679−686.
(45) Ding, F.; Yang, Y.; Deshpande, R. A.; Bozhevolnyi, S. I. A Review of Gap-Surface Plasmon Metasurfaces: Fundamentals and Applications. *Nanophotonics* **2018**, *7* (6), 1129−1156.
(46) Moreau, A.; Ciracì, C.; Mock, J. J.; Smith, D. R.; Hill, R. T.; Chilkoti, A.; Wang, Q.; Wiley, B. J. Controlled-Reflectance Surfaces with Film-Coupled Colloidal Nanoantennas. *Nature* **2012**, *492* (7427), 86−89.
(47) Lassiter, J. B.; McGuire, F.; Mock, J. J.; Ciracì, C.; Hill, R. T.; Wiley, B. J.; Chilkoti, A.; Smith, D. R. Plasmonic Waveguide Modes of Film-Coupled Metallic Nanocubes. *Nano Lett.* **2013**, *13* (12), 5866−5872.

https://doi.org/10.1021/acs.nanolett.1c04175
Nano Lett. 2022, 22, 3525−3531

(48) Chikkaraddy, R.; Zheng, X.; Benz, F.; Brooks, L. J.; De Nijs, B.; Carnegie, C.; Kleemann, M. E.; Mertens, J.; Bowman, R. W.; Vandenbosch, G. A. E.; Moshchalkov, V. V.; Baumberg, J. J. How Ultranarrow Gap Symmetries Control Plasmonic Nanocavity Modes: From Cubes to Spheres in the Nanoparticle-on-Mirror. *ACS Photonics* **2017**, *4* (3), 469−475.
(49) Akselrod, G. M.; Huang, J.; Hoang, T. B.; Bowen, P. T.; Su, L.; Smith, D. R.; Mikkelsen, M. H. Large-Area Metasurface Perfect Absorbers from Visible to Near-Infrared. *Adv. Mater.* **2015**, *27* (48), 8028−8034.
(50) Koethe, T. C.; Hu, Z.; Haverkort, M. W.; Schüßler-Langeheine, C.; Venturini, F.; Brookes, N. B.; Tjernberg, O.; Reichelt, W.; Hsieh, H. H.; Lin, H. J.; Chen, C. T.; Tjeng, L. H. Transfer of Spectral Weight and Symmetry across the Metal-Insulator Transition in VO_2. *Phys. Rev. Lett.* **2006**, *97* (11), 1−4.
(51) Morsy, A. M.; Barako, M. T.; Jankovic, V.; Wheeler, V. D.; Knight, M. W.; Papadakis, G. T.; Sweatlock, L. A.; Hon, P. W. C.; Povinelli, M. L. Experimental Demonstration of Dynamic Thermal Regulation Using Vanadium Dioxide Thin Films. *Sci. Rep.* **2020**, *10* (1), 13964.
(52) Kozen, A. C.; Joress, H.; Currie, M.; Anderson, V. R.; Eddy, C. R.; Wheeler, V. D. Structural Characterization of Atomic Layer Deposited Vanadium Dioxide. *J. Phys. Chem. C* **2017**, *121* (35), 19341−19347.
(53) Currie, M.; Mastro, M. A.; Wheeler, V. D. Characterizing the Tunable Refractive Index of Vanadium Dioxide. *Opt. Mater. Express* **2017**, *7* (5), 1697.
(54) Currie, M.; Mastro, M. A.; Wheeler, V. D. Atomic Layer Deposition of Vanadium Dioxide and a Temperature-Dependent Optical Model. *J. Vis. Exp.* **2018**, *2018* (135), e57103.
(55) Kinkhabwala, A.; Yu, Z.; Fan, S.; Avlasevich, Y.; Müllen, K.; Moerner, W. E. Large Single-Molecule Fluorescence Enhancements Produced by a Bowtie Nanoantenna. *Nat. Photonics* **2009**, *3* (11), 654−657.

https://doi.org/10.1021/acs.nanolett.1c04175
Nano Lett. 2022, 22, 3525−3531